

COMPUTING THE FINAL EPIDEMIC SIZE DISTRIBUTIONS OF A MULTI-TYPE GALTON–WATSON PROCESS

BY YUTA OKADA^{1,a} AND HIROSHI NISHIURA^{1,b}

¹*School of Public Health, Graduate School of Medicine, Kyoto University, okada.yuta.4y@kyoto-u.ac.jp;*

^b*nishiura.hiroshi.5r@kyoto-u.ac.jp*

The Galton–Watson process (GWP) is a discrete-time branching process model that provides a powerful tool for analyzing epidemic data and estimating key epidemiological parameters such as the basic reproduction number. When used with surveillance-based cluster size data, the GWP can also elicit information about the extent of transmission heterogeneity, even when each transmission process is not directly observable. When cluster size distribution data are available, the parameters that govern the transmission can be statistically inferred by using the probability mass function that corresponds to the observed cluster size data. For multi-type GWPs, however, real-world applications remain limited, possibly because of the absence of conceptually and practically straightforward approaches for deriving the closed-form solution of the final size distribution. In the present study, we propose a framework for computing the final size distribution of multi-type GWPs, using a method for the choice of the Cauchy integral contour. We provide examples of how our framework can be applied to both simulated data and real-world data of Middle East respiratory syndrome, and discuss potential pitfalls surrounding the identifiability of parameters for statistical inference when using likelihoods that are not conditioned on extinction.

1. Introduction. Stochastic epidemic models have been studied both as a mathematical description of the epidemic process and as a robust tool for statistical inference. Depending on the scientific question, setting of interest, or the availability of data, these models have been applied not only to analysis of the real-time transmission dynamics, but also to the demonstration of the heterogeneous nature of transmission and the determination of the eventual size of epidemics. The eventual (or asymptotic) distribution of the risk of infection is a key focus of research because of its practical importance from a public health perspective. Numerous studies have explored the theory surrounding the basic reproduction number and asymptotic state of epidemics as a stochastic process in a closed population with a social or network structure (Ball, 1986; Lefevre and Picard, 1990; Scalia-Tomba, 1990; Pellis, Ball and Trapman, 2012; Allard et al., 2009; Kenah and Robins, 2007). Considering an infinitely large closed population, which may be valid during the early epidemic period, the epidemic process is well approximated by branching process models, the theoretical properties of which have been extensively studied (Harris, 1963; Athreya and Ney, 1972). The Galton–Watson process (GWP), which is a discrete-time, memory-less branching process, has been applied to epidemic cluster size distribution data for the statistical inference of key epidemiological quantities including the basic reproduction number and the degree of transmission heterogeneity (e.g., the dispersion parameter of the negative binomial distribution) (Gay et al., 2004; Blumberg and Lloyd-Smith, 2013a,b; Blumberg, Funk and Pulliam, 2014; Nishiura et al., 2015; Kucharski and Althaus, 2015; Kucharski and Edmunds, 2015; Endo et al., 2020; Tran-Kiem and Bedford, 2024; Hodcroft et al., 2025).

Keywords and phrases: Multi-type branching process, Galton–Watson process, Epidemics, Final size, Cauchy integral.

The application of single-type GWPs to epidemic cluster size data is facilitated by the fact that the explicit form of the final size distribution for a negative binomial offspring is known and can be directly used for likelihood-based statistical inference. This use of GWPs has contributed to the statistical inference of epidemiological parameters, providing a foundation for evaluating the extinction probability of epidemics. Recent studies have proposed approaches for extending this conventional extinction probability to the real-time prediction and forecasting of epidemics (Lee and Nishiura, 2019; Bradbury et al., 2023; Hart et al., 2024). In reality, however, transmission depends on host attributes such as age, susceptibility, and contact behavior; therefore, beyond the single-type GWP, a multi-type specification becomes more desirable for the design of targeted (i.e., risk-based) public health interventions, such as age- or host-specific countermeasures.

While several studies have focused on the eventual extinction or containment probabilities for multi-type branching processes (Spencer and O’Neill, 2011), there has been limited research on the practical application of the likelihood-based inference of epidemiological parameters by calculating the final sizes for multi-type GWPs. Existing methods for calculating the final size distribution fall into the following categories:

1. Symbolic iteration of the final size probability generating functions (PGFs) or algebraic evaluation of the final size PGF (Brummitt, D’Souza and Leicht, 2012; Qi, Ju and Sun, 2017).
2. Tree enumeration (Kucharski and Edmunds, 2015; Chaumont and Liu, 2015).
3. Numerical calculation of the Cauchy integral representation of the coefficients of the final size PGF (Brummitt, D’Souza and Leicht, 2012).

Regarding these categories, approach 1 is difficult to trace for general PGFs. Approach 2 has been successfully applied to epidemiological data (Kucharski and Edmunds, 2015) by assuming independent negative binomial distributions for all transmission pathways between the types of hosts and applying the known approach of Chaumont and Liu (Chaumont and Liu, 2015). One potential bottleneck of this approach is that the calculation of probabilities for each potential transmission pathway is not straightforward for general offspring distributions. Approach 3 is straightforward because it reduces to calculating the Cauchy integral representation of the PGF coefficients; this method can be applied to general forms of PGFs, which in itself is a widely used technique (in an epidemiological context, see Miller (2018); Roberts et al. (2023)). To the best of our knowledge, however, there has been no explicit description of a theory-backed criterion for choosing contours that ensures the validity of the Cauchy integral calculation regarding final size distributions. A discussion of this problem is given in Section 2. This issue was the motivation for the present study. Bearing in mind that the use of likelihoods conditioned on extinction makes it impossible to identify the criticality of the underlying process (Farrington, Kanaan and Gay, 2003; Waxman and Nouvellet, 2019; Jagers and Lagerås, 2008), we believe that an inference framework using the unconditional likelihood, which allows for seamless handling of the sub- and supercritical regimes, will prove to be useful. This is especially true when considering the uncertainty regarding criticality, which is a key factor in the context of public health risk assessment, particularly during the early epidemic period.

Given these backgrounds, the major focus of this paper is to propose a straightforward method for calculating the final size distribution of multi-type GWPs, which relies on the Cauchy integral representation of the coefficients of the PGF of the final size distribution. The remainder of this paper is organized as follows. Section 2 provides a brief introduction to the final size PGF of GWPs, and summarizes two key approaches for determining the final size PGFs based on a Cauchy integral calculation. We then present our contributions, which are threefold. First, Section 3 establishes a contour-selection result that guarantees

the existence and uniqueness of the solution to the multi-type final size fixed-point equation on the chosen contours, thereby providing a theoretical justification for directly calculating the final size PGF coefficient. Second, Section 4 presents a practical numerical procedure based on standard optimization and the discrete Fourier transformation. Third, Sections 5 and 6 provide illustrative examples of the final size calculation and its implementation in likelihood-based inference using simulated and real multi-type cluster size data. Section 7 highlights the potential mechanism that may cause the trade-off between mean transmission and dispersion in the supercritical domain, as observed in the results in Section 6.

2. Galton–Watson process and its final size. In this section, we briefly describe some general results regarding single- and multi-type GWPs, and the final size distributions that are expressed by functional equations of PGFs.

2.1. Single-type GWP. For a single-type GWP, the PGF of the underlying offspring distribution is generally written as

$$G(z) = \mathbb{E}[z^X] = \sum_{d \geq 0} p(d)z^d, \quad |z| \leq 1.$$

Generally, a GWP is classified by criticality according to its mean number of offspring: subcritical if $\frac{dG}{dz}(1) < 1$, critical if $\frac{dG}{dz}(1) = 1$, and supercritical if $\frac{dG}{dz}(1) > 1$ (Harris, 1963; Athreya and Ney, 1972). Given $G(z)$, the PGF of the final size (including the initial ancestor) $H(z)$ is (Harris, 1963)

$$(2.1) \quad H(z) = zG(H(z)), \quad |z| \leq 1,$$

which is also a power series of z . As mentioned in Section 1, the explicit form of $H(z)$ is known for negative binomial offspring in single-type GWPs, and has been applied in several studies (Nishiura et al., 2012; Blumberg and Lloyd-Smith, 2013a,b; Blumberg, Funk and Pulliam, 2014; Endo et al., 2020; Tran-Kiem and Bedford, 2024; Hodcroft et al., 2025).

2.2. Multi-type GWP. Analogously to Eq. (2.1), the PGF of the offspring originating from type i ($i = 1, 2, \dots, n$) of a multi-type GWP is generally written as

$$(2.2) \quad G^{(i)}(\mathbf{z}) = \mathbb{E} \left[\prod_j z_j^{X_{ij}} \right] = \sum_{d_1, \dots, d_n} p^{(i)}(d_1, \dots, d_n) z_1^{d_1} z_2^{d_2} \dots z_n^{d_n},$$

where $\mathbf{z} = (z_1, z_2, \dots, z_n)^\top \in \mathbb{C}^n$. The criticality of multi-type GWPs is defined by the spectral radius of the Jacobian matrix of $\mathbf{G}(\mathbf{z}) = (G^{(1)}(\mathbf{z}), \dots, G^{(n)}(\mathbf{z}))^\top$ at $\mathbf{z} = \mathbf{1}$, or

$$\mathbf{K} = \mathbf{J}_{\mathbf{G}}(\mathbf{1}) = \left[\frac{\partial G^{(i)}}{\partial z_j} \right]_{\mathbf{z}=\mathbf{1}}.$$

(In an epidemiological context, the general notation of next-generation matrices corresponds to \mathbf{K}^T .) The final size equation for the PGF of the GWP originating from a “parent” of type i is (Harris, 1963)

$$(2.3) \quad H^{(i)}(\mathbf{z}) = z_i G^{(i)}(H^{(1)}(\mathbf{z}), \dots, H^{(n)}(\mathbf{z})), \quad i = 1, \dots, n,$$

or

$$(2.4) \quad \mathbf{H}(\mathbf{z}) = \begin{pmatrix} H^{(1)}(\mathbf{z}) \\ \vdots \\ H^{(n)}(\mathbf{z}) \end{pmatrix} = \begin{pmatrix} z_1 & \dots & 0 \\ \vdots & \ddots & \vdots \\ 0 & \dots & z_n \end{pmatrix} \begin{pmatrix} G^{(1)}(\mathbf{H}(\mathbf{z})) \\ \vdots \\ G^{(n)}(\mathbf{H}(\mathbf{z})) \end{pmatrix} = \text{diag}(\mathbf{z})\mathbf{G}(\mathbf{H}(\mathbf{z})),$$

which we hereafter refer to as the “final size equation”.

2.3. *Cauchy integral-based calculation of final size distribution* . The coefficients of $H^{(i)}$ in Eq. (2.3) can be written as

(2.5)

$$\begin{aligned} f^{(i)}(d_1, \dots, d_n) &= \frac{1}{(2\pi i)^n} \oint_{\Gamma_z} \frac{H^{(i)}(z_1, \dots, z_n)}{z_1^{d_1+1} \dots z_n^{d_n+1}} dz_1 \dots dz_n \\ &= \frac{1}{(2\pi i)^n} \oint_{\Gamma_h} h_i \left[\prod_m \left(\frac{G^{(m)}(h_1, \dots, h_n)}{h_m} \right)^{d_m+1} \right] \det(\mathbf{J}_{z \rightarrow h}(\mathbf{h})) dh_1 \dots dh_n, \end{aligned}$$

where $\Gamma_z = C_{z_1} \times C_{z_2} \times \dots \times C_{z_n}$ and $\Gamma_h = C_{h_1} \times C_{h_2} \times \dots \times C_{h_n}$ are contours with respect to complex variables $\mathbf{z} = (z_1, z_2, \dots, z_n)$ and $\mathbf{h} = (h_1, h_2, \dots, h_n)$, respectively. The latter Cauchy integral is the Lagrange–Good formula (Good, 1960), which involves the change of variables from \mathbf{z} to \mathbf{h} ; the term $\det(\mathbf{J}_{z \rightarrow h}(\mathbf{h}))$ in the integrand is the determinant of the Jacobian matrix:

$$(2.6) \quad \mathbf{J}_{z \rightarrow h}(\mathbf{h}) = \left[\frac{\partial z_i}{\partial h_j} \right], \quad \frac{\partial z_i}{\partial h_j} = \frac{1}{G^{(i)}(\mathbf{h})} \left(\delta_{i,j} - \frac{\partial G^{(i)}}{\partial h_j} \frac{h_i}{G^{(i)}} \right),$$

where $\delta_{i,j}$ is the Kronecker delta.

An obvious advantage of calculating the final size distribution based on the Cauchy integral method in Eq. (2.5) is that the conceptual and practical representation is mathematically very straightforward. However, a criterion for valid choices of contours for the Cauchy integral calculation needs to be clarified. Namely, regarding the first integral of Eq. (2.5), the existence and uniqueness of $H^{(i)}(z_1, \dots, z_n)$ in the integrand do not readily follow, especially for supercritical processes: this is the key focus of the present study, and relevant analysis will follow. Regarding the second integral, the regularity of $\mathbf{J}(\mathbf{h})$ in the integrand should be guaranteed inside the contours, although there is only a general principle to choose “sufficiently small” radii for contours. Therefore, in Section 4, where this Lagrange–Good formula-based approach (LG-approach) will be used, we resort to a numerical approach to ensure applicability.

3. Solution to the final size equation for $z \in \mathbb{C}^n$. To evaluate the Cauchy integral representation of the final size PGF coefficient, we require a unique solution to Eq. (2.4) for every \mathbf{z} on the contour Γ_z . The following proposition shows the existence of such a contour.

PROPOSITION 3.1. *Let $\mathbf{G}(\mathbf{z}) = (G^{(1)}(\mathbf{z}), \dots, G^{(n)}(\mathbf{z}))^T$ be the offspring PGF vector of an n -type GWP defined for $|z_i| \leq 1$, $i = 1, 2, \dots, n$, such that $\mathbf{J}_{\mathbf{G}}(\mathbf{r})$ has finite elements and is nonnegative and irreducible for $\mathbf{r} \in (0, 1]^n$. Then, there exists $\mathbf{r}^\# = (r_1^\#, \dots, r_n^\#) \in [0, 1]^n$ such that, for every complex vector \mathbf{z} inside the polydisk $D_z : |z_i| < r_i^\#, i = 1, \dots, n$, the functional equation*

$$(3.1) \quad \mathbf{h} = \text{diag}(\mathbf{z})\mathbf{G}(\mathbf{h}) =: \mathbf{T}_z(\mathbf{h})$$

has a unique solution $\mathbf{h} \in \mathbb{C}^n$ with $|\mathbf{h}| \leq |\mathbf{z}| < \mathbf{r}^\#$.

PROOF SKETCH. Let $\mathbf{r} = |\mathbf{z}|$. For $\mathbf{h}, \mathbf{h}' \in \mathbb{C}^n$ such that $\mathbf{h} \neq \mathbf{h}'$ and $|\mathbf{h}|, |\mathbf{h}'| \leq \mathbf{r}$, for any $\mathbf{r} \in (0, 1)^n$, we may choose a positive vector $\mathbf{x} = \mathbf{x}(\mathbf{r})$ such that the following relationship holds for the infinity norms weighted by \mathbf{x} :

$$\|\mathbf{T}_z(\mathbf{h}') - \mathbf{T}_z(\mathbf{h})\|_{\infty, \mathbf{x}} \leq \|\text{diag}(\mathbf{r})\mathbf{J}_{\mathbf{G}}(\mathbf{r})\|_{\infty, \mathbf{x}} \|\mathbf{h}' - \mathbf{h}\|_{\infty, \mathbf{x}},$$

which can be seen from the fact that $\mathbf{J}_{\mathbf{G}}(\mathbf{z})$ (the Jacobian matrix of \mathbf{G} with respect to \mathbf{z}) has nonnegative power-series coefficients, and hence $\|\mathbf{J}_{\mathbf{G}}(\mathbf{z})\|_{\infty, \mathbf{x}} \leq \|\mathbf{J}_{\mathbf{G}}(|\mathbf{z}|)\|_{\infty, \mathbf{x}} = \|\mathbf{J}_{\mathbf{G}}(\mathbf{r})\|_{\infty, \mathbf{x}}$.

Then, there exists $\mathbf{r}^\# \in (0, 1)^n$ and a positive weight vector $\mathbf{x}^\# = \mathbf{x}(\mathbf{r}^\#)$ such that $\|\text{diag}(\mathbf{r}^\#)\mathbf{J}_G(\mathbf{r}^\#)\|_{\infty, \mathbf{x}^\#} < 1$. Briefly, for subcritical and critical processes, any $\mathbf{r}^\# \in (0, 1 - \epsilon)^n$ satisfies this condition. For supercritical processes, there exists $\mathbf{r}^\#$ such that $r_i^\# \in (q_i, 1), i = 1, \dots, n$, where $\mathbf{q} = (q_1, \dots, q_n)$ is the extinction probability vector, or the smallest positive root of $\mathbf{q} = \mathbf{G}(\mathbf{q})$.

Consequently, regardless of the criticality of the underlying GWP, we may choose contours inside a polydisk $D_{\mathbf{z}} : |z_i| < r_i^\#$ such that $\mathbf{T}_{\mathbf{z}}$ becomes a contraction mapping. This ensures not only the existence, but also the uniqueness of the solution to Eq. (3.1). (A full proof is provided in Section 1 of the Supplementary Material.) \square

The discussion in Proposition 3.1 essentially leads to a determination of the region of \mathbf{z} in which the derivatives of $\mathbf{H}(\mathbf{z})$ are finite (see Section 2 of the Supplementary Material).

Upon the practical implementation of Proposition 3.1, it is sufficient to ensure the condition $\rho(\text{diag}(\mathbf{r}^\#)\mathbf{J}_G(\mathbf{r}^\#)) < 1$. However, for simplicity, the following sections adopt the more conservative condition that $\rho(\mathbf{J}_G(\mathbf{r}^\#)) < 1$ for supercritical cases.

4. Numerical framework for calculating final size distributions. In this section, we briefly describe the numerical framework used to compute final size distributions. The framework itself is a combination of standard methods for calculating Cauchy integrals and for optimization, with adaptations based on what was discussed in Section 3.

4.1. Choice of Cauchy integral contours. The calculation of PGF coefficients using Cauchy integrals has previously been described in an epidemiological context (Miller, 2018; Roberts et al., 2023); we apply an analogous framework to multivariate settings. The computation of the coefficients of the final size PGF is based on a multivariate Cauchy integral:

$$(4.1) \quad f^{(i)}(d_1, \dots, d_n) = \frac{1}{(2\pi i)^n} \oint_{\Gamma_{\mathbf{z}}} \frac{H^{(i)}(z_1, \dots, z_n)}{z_1^{d_1+1} \dots z_n^{d_n+1}} dz_1 \dots dz_n,$$

which we evaluate on multidimensional grids along the contour $\Gamma_{\mathbf{z}} = C_{z_1} \times \dots \times C_{z_n}$ using the discrete Fourier transform (DFT) (Trefethen and Weideman, 2014). Here, each C_{z_j} is a circle defined by $|z_j| = r_j$.

The critical step enabled by Proposition 3.1 is the principled choice of the contour radii $\mathbf{r} = (r_1, \dots, r_n)$ to guarantee the existence and uniqueness of the integrand. To balance this theoretical requirement with general recommendations to minimize rounding and aliasing errors (Bornemann, 2011; Abate and Whitt, 1992), we construct the contour as follows:

- Subcritical or critical: $\mathbf{r} = (0.95, \dots, 0.95)$.
- Supercritical: We first find a vector $\mathbf{r}^\# = \mathbf{q} + t^\#(\mathbf{1} - \mathbf{q})$ with $t^\# \in (0, 1)$ such that $\rho(\mathbf{J}_G(\mathbf{r}^\#)) = 0.975$, which is a conservative threshold chosen to ensure a certain margin from the theoretical threshold. We then set $r_j = \min(r_j^\#, 0.95)$.

(The detailed formulation of the DFT approximation and the rule for determining the optimal grid size N are described in Section 3.1 of the Supplementary Material.)

4.2. Solving the final size equation on the contour. To evaluate the numerator of the integrand, i.e., $H^{(i)}(\mathbf{z})$ in Eq. (4.1), at each grid point via DFT, we must find the unique solution \mathbf{h} to Eq. (3.1) for every \mathbf{z} on $\Gamma_{\mathbf{z}}$. This is equivalent to finding roots of the system

$$(4.2) \quad \mathbf{F}_{\mathbf{z}}(\mathbf{h}) = \mathbf{h} - \text{diag}(\mathbf{z})\mathbf{G}(\mathbf{h}) = \mathbf{0}.$$

We solve this equation as a minimization problem of $\psi_{\mathbf{z}}(\mathbf{h}) = \|\mathbf{F}_{\mathbf{z}}(\mathbf{h})\|_2^2$, or the product of $\mathbf{F}_{\mathbf{z}}(\mathbf{h})$ and its conjugate transpose, by using a numerical approach based on Newton's

method with backtracking (Nocedal and Wright, 2006). Proposition 3.1 ensures both the existence of a unique solution and the regularity of the Jacobian matrix $\mathbf{J}_{F_z}(\mathbf{h})$ within the region $|\mathbf{h}| \leq r^\#$, thus guaranteeing the convergence of an arbitrary Newton sequence starting from $|\mathbf{h}| \leq r^\#$. (Details are provided in Section 3.2 of the Supplementary Material.)

Once the unique solution \mathbf{h} has been computed for all grids for z on the contour, these shared values can be efficiently reused to calculate the entire probability mass matrix.

5. Case study on simulated data. In this section, we illustrate the application of our framework on hypothetical offspring distributions and simulated datasets. As an example, we assume a two-type GWP with negative multinomial offspring distributions.

5.1. *Comparison with the Lagrange–Good method.* First, to compare the performance of the final size PGF calculation given by the LG approach with that of ours, we build the underlying 2×2 mean offspring matrix $\mathbf{K} = \left[\frac{\partial G^{(i)}}{\partial z_j} \right]_{z=1}$ using three scalars (R, α, p) , where $R > 0$ and $\alpha, p \in [0, 1]$. We first define the skeleton matrix as

$$(5.1) \quad \mathbf{B}(\alpha, p) = \begin{pmatrix} \alpha p & \alpha(1-p) \\ (1-\alpha)(1-p) & (1-\alpha)p \end{pmatrix},$$

in which the row sums are α and $1 - \alpha$, respectively. Here, α controls the relative expected number of secondary cases generated by type 1 versus type 2 primary cases, whereas p controls the within-type transmission probabilities for the two types. We then scale \mathbf{B} so that the spectral radius of \mathbf{K} is equal to the reproduction number R :

$$(5.2) \quad \mathbf{K} = R \frac{\mathbf{B}}{\rho(\mathbf{B})} = \begin{pmatrix} K_{11} & K_{12} \\ K_{21} & K_{22} \end{pmatrix},$$

where $\rho(\cdot)$ denotes the spectral radius of an arbitrary matrix. We model the offspring vector using a negative multinomial PGF:

$$(5.3) \quad G^{(i)}(z_1, z_2; \boldsymbol{\theta}) = \left(1 + \frac{1}{k} \sum_{j=1}^2 K_{ij} (1 - z_j) \right)^{-k}, \quad i = 1, 2,$$

where $k > 0$ is the dispersion parameter and $\boldsymbol{\theta} = (R, \alpha, p, k)$. Other than the choice of contour radii, the calculation of the PGF coefficients using this LG approach proceeds in the same manner as described in Section 4. (Details on the choice of contour radii for the LG-based approach are provided in Section 4 of the Supplementary Material.)

Table 1 summarizes the parameter values used to specify $G^{(i)}$ and the metrics used to compare the LG-based approach with our approach. We evaluate the final size distribution for total secondary cases ≤ 40 for each type. The results in Table 1 indicate that our approach and the LG-based approach yield almost the same results, with very minor absolute differences. With the calculation of probability mass up to the maximum degree of 40 for the two host types, the total probability mass is close to the extinction probability, which is to be expected if the calculation is performed correctly.

5.2. *Likelihood surface for a simulated dataset.* We now demonstrate the likelihood surface captured by our proposed approach, with the aim of showing that the smoothness spans the criticality threshold. For this purpose, we simulate cluster data based on the contact matrix used in a previous study (Kucharski and Edmunds, 2015) that considered a two-type process, where type 1 represents individuals aged < 20 years and type 2 represents those aged ≥ 20 years. Let \mathbf{M} be a 2×2 contact matrix, where m_{ij} denotes the average number of contacts

TABLE 1

Numerical comparison between the proposed method and the Lagrange–Good (LG) implementation (max degree: 40 for each type).

R	k	α	p	index i	Q_i	sum(LG)	sum(current)	max abs diff
0.50	0.1	0.25	0.25	1	1.0000	0.9993	0.9993	3.4×10^{-12}
				2	1.0000	0.9978	0.9978	4.6×10^{-12}
0.50	0.1	0.25	0.75	1	1.0000	0.9998	0.9998	1.6×10^{-12}
				2	1.0000	0.9971	0.9971	5.0×10^{-12}
0.50	1	0.25	0.25	1	1.0000	1.0000	1.0000	3.5×10^{-12}
				2	1.0000	1.0000	1.0000	8.5×10^{-12}
0.50	1	0.25	0.75	1	1.0000	1.0000	1.0000	2.6×10^{-13}
				2	1.0000	0.9999	0.9999	6.6×10^{-12}
1.25	0.1	0.25	0.25	1	0.9749	0.9655	0.9655	4.1×10^{-12}
				2	0.9521	0.9338	0.9338	4.4×10^{-12}
1.25	0.1	0.25	0.75	1	0.9917	0.9870	0.9870	5.3×10^{-12}
				2	0.9589	0.9389	0.9389	4.4×10^{-12}
1.25	1	0.25	0.25	1	0.8705	0.8647	0.8647	3.2×10^{-10}
				2	0.7540	0.7431	0.7431	5.3×10^{-10}
1.25	1	0.25	0.75	1	0.9568	0.9539	0.9539	1.8×10^{-11}
				2	0.7878	0.7736	0.7736	6.0×10^{-11}

that a type- j individual makes with type- i individuals. As a fixed “skeleton” mixing pattern, we use the following matrix aggregated into the two age groups:

$$(5.4) \quad \mathbf{M} = \begin{pmatrix} 4.3 & 3.0 \\ 1.3 & 2.7 \end{pmatrix}.$$

Using \mathbf{M} normalized by its spectral radius, the mean offspring matrix is modeled as

$$(5.5) \quad \mathbf{K}(R) = R \left(\frac{\mathbf{M}}{\rho(\mathbf{M})} \right)^T,$$

where $\rho(\mathbf{K}(R)) = R$. Based on this matrix, we construct a negative multinomial PGF in the same manner as in Eq. (5.3), with a common dispersion parameter k for the two types. Upon simulation, we arbitrarily assume that independent clusters with $(n_1, n_2) = (20, 20)$ for both types of index cases have been observed. For this demonstration, we arbitrarily produce this dataset by assuming $R = 0.75, k = 0.1$ (details can be found in Section 5 of the Supplementary Material).

A two-dimensional plot of the likelihood surface at the maximum likelihood estimate (MLE; $R = 0.578, k = 0.211$) is drawn in the left panel of Figure 1, where the horizontal axis represents $\log R$ and the vertical axis represents $\log k$. (The MLE for a single finite simulated dataset is not expected to coincide exactly with the underlying parameter values used for data generation.) First, the likelihood is smoothly connected across the criticality threshold $\log(R) = 0$. Second, the contours exhibit a bifurcating shape: in the subcritical region ($R \leq 1$), they form a ridge extending from the bottom-left towards the MLE, indicating a positive correlation between R and k . In contrast, in the supercritical region ($R > 1$), the contour shows a pronounced ridge extending toward the bottom-right (larger R and smaller k). This descending ridge is naturally interpreted as a trade-off that stems from the extinction probabilities, which may possibly reflect an inherent identifiability challenge. In Section 7, we discuss a hypothesis on the mechanism underlying this supercritical ridge and its connection to the results in Section 6.

6. Case study: MERS cluster size data from 2012–13.

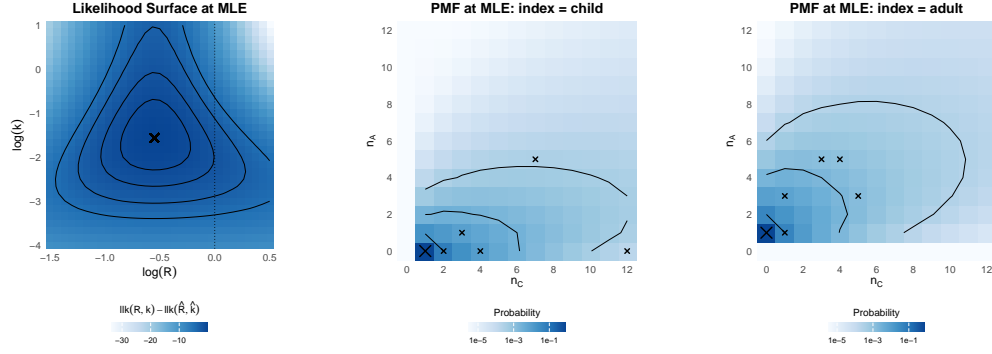


FIG 1. Likelihood surface and estimated probability mass functions (PMFs) for the simulated two-type transmission cluster data. (Left) Two-dimensional likelihood surface for the reproduction number R and dispersion parameter k in log-scale. The horizontal axis represents $\log R$ and the vertical axis represents $\log k$. The black crosses indicate the maximum likelihood estimate (MLE). (Middle and Right) Observed cluster sizes (black crosses) overlaid on the predicted final size PMFs for transmission chains originating from child and adult index cases, respectively, evaluated at the MLE.

6.1. *Dataset and methods.* In this section, we discuss how our framework operates by applying it to the Middle East respiratory syndrome (MERS) dataset in Cauchemez et al. (2014), which was later revisited in Kucharski and Edmunds (2015). This dataset consists of 42 clusters involving 111 confirmed human cases, with information on the age group (< 20 vs. ≥ 20 years) and the index case for each cluster. For some transmission clusters, category information (children or adults) is lacking for cases that include the index cases. We consider a two-type GWP in which type 1 and type 2 represent individuals aged < 20 years and ≥ 20 years, respectively, following the structure in Kucharski and Edmunds (2015).

For an infectious individual of type $i \in \{1, 2\}$, let (X_{i1}, X_{i2}) denote the numbers of secondary cases in the two age groups. The PGF of an offspring starting from type i can be written as $G^{(i)}(z_1, z_2; \boldsymbol{\theta}) = \mathbb{E}[z_1^{X_{i1}} z_2^{X_{i2}}]$, $|z_1| < 1, |z_2| < 1$, where $\boldsymbol{\theta}$ are GWP parameters that will be fully described later. Following Kucharski and Edmunds (2015), we use the following next-generation matrix:

$$(6.1) \quad R \frac{SM}{\rho(SM)} = \lambda \begin{pmatrix} 1 & 0 \\ 0 & s \end{pmatrix} \begin{pmatrix} m_{11} & m_{12} \\ m_{21} & m_{22} \end{pmatrix} (= \mathbf{K}^T),$$

where $S = \text{diag}(1, s)$ expresses the relative susceptibility of adults compared with children ($s < 1$ is assumed, as in Kucharski and Edmunds (2015)), $\mathbf{M} = (m_{ij})$ is the contact matrix, and λ is a scalar. Following this formulation, the negative multinomial PGF $G^{(i)}$ is defined as

$$(6.2) \quad G^{(i)}(z_1, z_2; \boldsymbol{\theta}) = \left(1 + \frac{1}{k} \sum_{j=1}^2 K_{ij} (1 - z_j) \right)^{-k}, \quad i = 1, 2.$$

The final size PGF of the transmission chain originating from a single index case of type i satisfies

$$(6.3) \quad H^{(i)}(z_1, z_2; \boldsymbol{\theta}) = z_i G^{(i)}(H^{(1)}(z_1, z_2; \boldsymbol{\theta}), H^{(2)}(z_1, z_2; \boldsymbol{\theta})), \quad i = 1, 2.$$

For an arbitrary cluster dataset $D = \{i, d_1, d_2\}$ (where the index case is type i and the numbers of type 1 and type 2 cases are d_1 and d_2 , respectively), we may calculate $p_i(d_1, d_2; \boldsymbol{\theta}) = [z_1^{d_1} z_2^{d_2}] H^{(i)}(z_1, z_2; \boldsymbol{\theta})$, the coefficient of $z_1^{d_1} z_2^{d_2}$ in $H^{(i)}$.

Let $I_D \in \{1, 2, \text{NA}\}$ denote the recorded type of the index case in cluster D , where $I_D = \text{NA}$ indicates that the index type information is missing from the report. By considering $p(I_D = 1) = \pi$, i.e., the probability that a reported cluster starts from an index case with type 1, and $p(I_D = 2) = 1 - \pi$, the likelihood of observing the cluster can be simply written as $L_D = p(I_D = i)p_i(d_1, d_2; \boldsymbol{\theta})$, $i = 1, 2$, for datasets with complete information on the type of both the index case and all cases.

When complete information on the type of index case or type information for some cases is lacking, as for some clusters in the MERS dataset, some additional consideration is required.

A) The type of the index case is unknown ($I_D = \text{NA}$), but complete information is available for the types of all cases: By considering π , i.e., the probability that a reported cluster starts from an index case of type 1, the marginalized likelihood of observing the cluster is

$$(6.4) \quad L_D = \sum_{i=1}^2 p(I_D = i)p_i(d_1, d_2; \boldsymbol{\theta}) = \pi p_1(d_1, d_2; \boldsymbol{\theta}) + (1 - \pi)p_2(d_1, d_2; \boldsymbol{\theta}).$$

B) The type of the index case is known, but there is incomplete information on the types for all cases in the cluster: When the type of the index case is known to be type i , the marginal likelihood of observing the cluster can be calculated as

$$(6.5) \quad L_D = p(I_D = i) \sum_{m=0}^M p_i(d_1^{\text{obs}} + m, d_2^{\text{obs}} + M - m; \boldsymbol{\theta}),$$

where M is the total number of cases in the cluster whose exact type is unknown (i.e., $M = N_{\text{total}} - d_1^{\text{obs}} - d_2^{\text{obs}}$).

C) Both the type of the index case and complete information on all cases are missing: By analogy to the preceding two cases, the marginalization is

$$(6.6) \quad L_D = \sum_{m=0}^M \left(\pi p_1(d_1^{\text{obs}} + m, d_2^{\text{obs}} + M - m; \boldsymbol{\theta}) + (1 - \pi)p_2(d_1^{\text{obs}} + m, d_2^{\text{obs}} + M - m; \boldsymbol{\theta}) \right).$$

Following scenarios A–C, we may calculate the total likelihood for observing the entire dataset of MERS clusters as

$$(6.7) \quad L(\boldsymbol{\theta}) = \prod_{D \in D_{\text{MERS}}} L_D(\boldsymbol{\theta}),$$

where $\boldsymbol{\theta} = \{\log R, \log k, \text{logit } S, \text{logit } \pi\}$. For $\boldsymbol{\theta}$, weakly informative priors are introduced for statistical inference:

$$(6.8) \quad \begin{aligned} \log(R) &\sim \text{Normal}(0, 1^2), \\ \log(k) &\sim \text{Normal}(0, 2^2), \\ \text{logit}(S) &\sim \text{Normal}(0, 5^2), \\ \text{logit}(\pi) &\sim \text{Normal}(0, 5^2). \end{aligned}$$

We estimated the parameters using the Markov Chain Monte Carlo (MCMC) method, as implemented by the Differential Evolution MCMC algorithm (named “DEzs”) in the R package “BayesianTools” (Hartig, Minunno and Paul, 2017) with four independent MCMC runs using three internal parallel subchains with 2,000 iterations. After discarding the first 1,000 iterations for each subchain, convergence was assessed and it was confirmed that all parameters satisfied $\hat{R} < 1.04$ and the effective sample size was > 770 . For convenience, we retained 1,200 posterior draws for every parameter to evaluate the model fit (additional diagnostic plots are provided in Figs. S1–S3 of the Supplementary Material).

TABLE 2
Parameters estimated from the MERS dataset.

Parameter	Posterior Median (95% CrI)
R	0.77 (0.57, 1.08)
k	0.30 (0.10, 1.20)
S	0.99 (0.89, 1.00)
π	0.05 (0.01, 0.14)

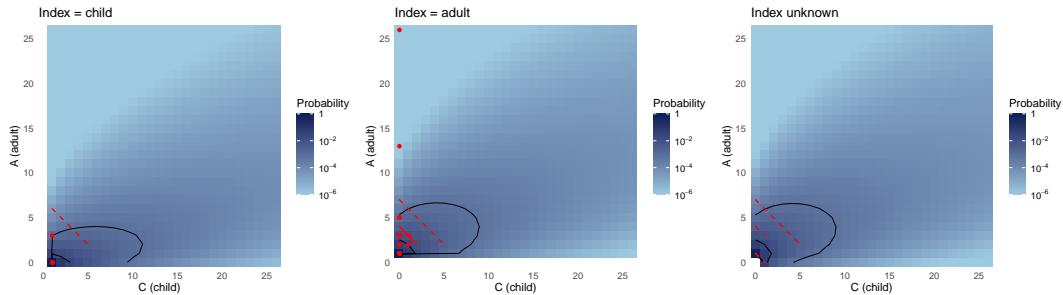


FIG 2. Posterior mean probability mass functions for observed child/adult cluster sizes under the fitted model. Black contours indicate the 50%, 80%, and 95% highest-mass regions. Dots denote clusters with fully observed child/adult counts. Solid line segments denote clusters with known index type, but incomplete child/adult composition, and dashed line segments denote clusters with unknown index type.

6.2. *Results.* The parameter estimates are presented in Table 2. The R estimate is 0.77 (95% CrI: 0.57, 1.08), which is comparable to that of Kucharski and Edmunds (2015). We did not specifically impose a constraint on R that forced the process to be subcritical, as can be observed in the posterior draws and uncertainty bound of R . The values of k , S , and π are estimated to be 0.30 (95% CrI: 0.10, 1.20), 0.99 (95% CrI: 0.89, 1.00), and 0.05 (95% CrI: 0.01, 0.14), respectively, where the estimated values of S are in line with previous estimates (Kucharski and Edmunds, 2015). As shown in Figure S3 in the Supplementary Material, the correlation between posterior samples suggests a ridge toward the high $\log R - \log k$ direction that extends into the supercritical domain.

Figure 2 confirms the fit of our inference results to the observed data by overlaying the observed clusters on the posterior mean probability mass matrix. Although it is difficult to make a clear judgement on whether or not the clusters with incomplete information are actually inside the 95% highest-mass region, only 2 out of 42 clusters are clearly outside that range.

7. Identifiability and parameter correlation in supercritical domains. We now explore the potential mechanism for the negative correlation between R and k for posterior draws in the supercritical ($R > 1$) region, as observed in the previous section. In general, the unconditional likelihood of observing cluster size data in general can be decomposed as

$$(7.1) \quad L_{\text{unconditional}}(\mathbf{D}; \boldsymbol{\theta}) = L_{\text{conditional}}(\mathbf{D}; \boldsymbol{\theta}) \times \prod_i q_i(\boldsymbol{\theta})^{n_i},$$

where \mathbf{D} denotes an arbitrary observation, n_i denotes the number of clusters observed in \mathbf{D} that originated from a type- i host, and q_i is the extinction probability for $i = 1, \dots, n$. For a subcritical GWP, the second term of Eq. (7.1) is trivial because $q_i = 1$, and it is known that $L_{\text{conditional}}(\mathbf{D}; \boldsymbol{\theta})$ does not have sufficient information to distinguish the criticality (Farrington, Kanaan and Gay, 2003; Waxman and Nouvellet, 2019; Jagers and Lagerås, 2008). Therefore, we may reasonably focus our discussion on the nontrivial q_i of supercritical GWPs. For

clarity and simplicity, we again consider negative multinomial offspring:

$$(7.2) \quad G^{(i)}(\mathbf{z}; \boldsymbol{\theta}) = \left(1 + \frac{1}{k_i} \sum_{j=1}^n K_{ij} (1 - z_j) \right)^{-k_i}, \quad i = 1, 2, \dots, n,$$

where k_i is the dispersion parameter, and focus on the fixed-point equation $\mathbf{q} = \mathbf{G}(\mathbf{q})$ that gives the extinction probability vector $\mathbf{q} = (q_1, \dots, q_n)^\top \in (0, 1)^n$. Both \mathbf{G} and \mathbf{q} are implicit functions of $\boldsymbol{\theta} = (\mathbf{K}, \mathbf{k})$, where $\mathbf{K} = (K_{ij})$ and $\mathbf{k} = (k_1, \dots, k_n)$. A small change in \mathbf{q} can be written as

$$(7.3) \quad dq_i = \sum_{\boldsymbol{\theta}} \frac{\partial q_i}{\partial \boldsymbol{\theta}} d\boldsymbol{\theta} = \sum_{j, \ell} \frac{\partial q_i}{\partial K_{j\ell}} dK_{j\ell} + \sum_j \frac{\partial q_i}{\partial k_j} dk_j, \quad i, j, \ell = 1, 2, \dots, n.$$

From the implicit differentiation of the fixed-point equation $\mathbf{q} = \mathbf{G}(\mathbf{q})$ (details are provided in the Supplementary Material), the following holds:

- $\frac{\partial q_i}{\partial K_{j\ell}} < 0$ for all i, j, ℓ ,
- $\frac{\partial q_i}{\partial k_j} < 0$ for all i, j .

Therefore, in general, implicit differentiation suggests a possible local trade-off among the parameters in $\boldsymbol{\theta}$ regarding $d\mathbf{q} \approx \mathbf{0}$. In the MERS setting in Section 6, where the mean offspring matrix is mostly anchored by the contact matrix, this is consistent with the negative association between $R = \rho(\mathbf{J}_G(\mathbf{1}))$ and k suggested by the ridge toward the bottom-right in the posterior correlation plot of $\log(R) - \log(k)$. However, this argument concerns only the trade-off regarding $d\mathbf{q} \approx \mathbf{0}$, and does not consider the change of $L_{\text{conditional}}(\mathbf{D}; \boldsymbol{\theta})$ in Eq. (7.1). Additionally, the region of interest in the supercritical domain will in principle approach the criticality threshold as the number of observed clusters increases. Nonetheless, for a given dataset, Eq. (7.1) indicates that this trade-off may potentially lead to parameter identifiability issues.

8. Discussion. The present study has focused on a practical framework for employing the Cauchy integral method to compute the final size PGFs of multi-type GWPs. First, our proof of Proposition 3.1 provided a theoretical basis for the valid computation of final size distributions via a Cauchy integral calculation, regardless of the criticality of the underlying GWP. Second, our simple scheme for calculating the final size distribution using a combination of Newton's method and DFT proved to be comparable to the LG approach when applied to simulated datasets, and enabled likelihood-based inference of key epidemiological parameters when applied to the MERS cluster size distribution data. In addition to our findings regarding practical implementation, we also explored possible parameter identifiability issues in the supercritical domain regarding the elements of the mean offspring matrix and overdispersion parameters for GWPs with negative multinomial offspring.

Several findings from the present study should be stressed. Regarding Proposition 3.1, our proof is essentially an application of contraction theory; however, to the best of our knowledge, practically feasible choices of contours in Cauchy integrals, as in Eq. (4.1), and the uniqueness of solutions to the final size formula of Eq. (3.1) on the entire contour under that choice have not been explicitly argued. In the present study, we clarified that, even when the underlying GWP is supercritical, there is an upper limit of suitable radii for contours that are greater than the extinction probability vector. Although we may adopt a more conservative condition upon application for simplicity, this may provide potential options when greater radii should be chosen for reasons of numerical stability. Another value of our approach is that it provides a firm basis for obtaining the numerator of the integrand in Eq. (4.1); this

has been applied in practice without explicit discussion on the convergence or uniqueness of solutions.

Technically, given that the performances of our approach and the LG-based approach were found to be comparable, there are two advantages of our approach over the LG-based approach. First, our approach does not involve the change of variables required in the LG method, and the principle for choosing the contours of the Cauchy integral is well-defined. Though it is possible to numerically examine the regularity of the Jacobian matrix appearing in the LG formula inside the contours (as we actually did in our demonstration), the principle is not well-defined in a practical sense. The second advantage is that, in our approach, the same h in the numerator of the integrand can be used for every PMF to be calculated; in the LG method, the integrands do not have common structures across different probability masses or PGF coefficients. This is important upon calculation of the entire probability mass matrices, for example, when we want to project the range of future numbers of cases for public health risk assessment purposes.

From a practical viewpoint, the final size distributions of multi-type GWPs have not been applied rigorously to real-world data, including epidemic cluster sizes, with limited applications based on tree enumeration or the Cauchy integral-based method (Brummitt, D'Souza and Leicht, 2012; Kucharski and Edmunds, 2015). In this context, our framework will serve not only as a theoretical foundation for the direct calculation of coefficients using Cauchy integrals, but also as an important addition to the conventional approaches because of its conceptual and practical simplicity, which may potentially promote wider application. Specifically, it is applicable to multi-type GWPs with general offspring PGFs not limited to the negative binomial or negative multinomial family, does not require numerical exploration of the regularity of the Jacobian as appears in the LG formula, and allows seamless handling of subcritical and supercritical processes within the same framework. It is also encouraging that we could actually infer epidemiological parameters without imposing an assumption on the criticality of the underlying GWP from both our simulated data and the MERS cluster size data.

Finally, we have revealed that extinction probabilities for GWPs with negative multinomial offspring are monotonically decreasing functions of both the elements of the mean offspring matrix and the overdispersion parameters for all types of hosts. In our context, the interpretation is that this may be the underlying mechanism of the negatively correlated $\log R$ and $\log k$ in the supercritical domain in our MERS result; however, our analysis provides a direct foundation behind the general notion regarding the effect that the reproduction number and the overdispersion parameter have on the extinction probability, as has been discussed for single-type processes (Lloyd-Smith et al., 2005).

Several limitations and extensions merit further investigation. First, our numerical algorithm was only tested for two host types. For greater numbers of host types, efficient computation in the higher-dimensional complex spaces should be considered, such as sparse approximations of the offspring PGFs or importance sampling in the complex space for efficient calculation of Cauchy integrals. Second, the case studies of our framework described in this paper only assumed negative multinomial offspring and did not incorporate information on how the clusters arise and are reported in the real world. Therefore, model misspecification or unobserved confounding factors may have biased our inference. Third, we did not specifically focus on the identifiability of the criticality itself, which is a recognized topic (Farrington, Kanaan and Gay, 2003; Waxman and Nouvellet, 2019). Exploring methods or datasets that may improve the identification of criticality will be an important direction for future work. Finally, we have focused on estimating the spectral radius of the mean offspring matrix and the overdispersion parameter from cluster size data. Extending the framework to real-time forecasting or to joint inference on additional epidemiological parameters, such as

generation-interval distributions or time-varying control measures, is an interesting direction for future work.

In conclusion, we have provided a straightforward framework for evaluating Cauchy integral representations of final size PGF coefficients for the multi-type GWP, with a practical guide for choosing valid contours of the Cauchy integrals. We also demonstrated the applicability of our framework both to simulated and real-world epidemiological data, while also providing an insight into the relationship between extinction probabilities and key epidemiological parameters, and its potential effect on parameter identifiability regarding statistical inference.

Acknowledgments. Hiroshi Nishiura is also affiliated with the Center for Health Security, Graduate School of Medicine, Kyoto University.

This work was supported by JSPS KAKENHI (grant number 25K20599 to YO), the Japan Agency for Medical Research and Development (grant number JP26fk0108742 to YO), the SECOM Science and Technology Foundation (YO), Health and Labour Sciences Research Grants (grant numbers 23HA2005 to HN), HU-RIZONT international research excellence program (Rapid-GRIP project: 2024-1.2.3-HU-RIZONT-2024-00034 to HN), the World Health Organization (HN), the Japan Science and Technology Agency CREST program (grant number JPMJCR24Q3 to HN). The funders had no role in the study design, data collection and analysis, decision to publish, or preparation of the manuscript.

We thank Stuart Jenkinson, PhD, from Edanz (<https://jp.edanz.com/ac>) for editing a draft of this manuscript.

SUPPLEMENTARY MATERIAL

Supplementary material for “Computing the final epidemic size distributions of a multi-type Galton–Watson process”

The supplement contains the full proof of Proposition 3.1, additional numerical details for the Cauchy integral and Lagrange–Good calculations, extra simulation results, MCMC diagnostics for the MERS analysis, and derivations for the sensitivity of extinction probabilities under negative multinomial offspring.

Code and data for reproducing the numerical results

This archive contains the R scripts and input data, together with key results in the article and supplement. These are also available at GitHub (URL: https://github.com/pk2393/FSD_calc_GWP) and Zenodo (URL: <https://doi.org/10.5281/zenodo.20446753>).

REFERENCES

- ABATE, J. and WHITT, W. (1992). The Fourier-series method for inverting transforms of probability distributions. *Queueing Syst.* **10** 5–87.
- ALLARD, A., NOËL, P.-A., DUBÉ, L. J. and POURBOHLOUL, B. (2009). Heterogeneous bond percolation on multitype networks with an application to epidemic dynamics. *Phys. Rev. E Stat. Nonlin. Soft Matter Phys.* **79** 036113.
- ATHREYA, K. B. and NEY, P. E. (1972). *Branching processes*, 1972 ed. *Grundlehren der mathematischen Wissenschaften*. Springer, Berlin, Germany.
- BALL, F. (1986). A unified approach to the distribution of total size and total area under the trajectory of infectives in epidemic models. *Advances in Applied Probability* **18** 289–310.
- BLUMBERG, S., FUNK, S. and PULLIAM, J. R. C. (2014). Detecting differential transmissibilities that affect the size of self-limited outbreaks. *PLoS Pathog.* **10** e1004452.
- BLUMBERG, S. and LLOYD-SMITH, J. O. (2013a). Comparing methods for estimating R_0 from the size distribution of subcritical transmission chains. *Epidemics* **5** 131–145.

- BLUMBERG, S. and LLOYD-SMITH, J. O. (2013b). Inference of $R(0)$ and transmission heterogeneity from the size distribution of stuttering chains. *PLoS Comput. Biol.* **9** e1002993.
- BORNEMANN, F. (2011). Accuracy and stability of computing high-order derivatives of analytic functions by Cauchy integrals. *Found. Comput. Math.* **11** 1–63.
- BRADBURY, N. V., HART, W. S., LOVELL-READ, F. A., POLONSKY, J. A. and THOMPSON, R. N. (2023). Exact calculation of end-of-outbreak probabilities using contact tracing data. *J. R. Soc. Interface* **20** 20230374.
- BRUMMITT, C. D., D’SOUZA, R. M. and LEICHT, E. A. (2012). Suppressing cascades of load in interdependent networks. *Proc. Natl. Acad. Sci. U. S. A.* **109** E680–9.
- CAUCHEMEZ, S., FRASER, C., VAN KERKHOVE, M. D., DONNELLY, C. A., RILEY, S., RAMBAUT, A., ENOUF, V., VAN DER WERF, S. and FERGUSON, N. M. (2014). Middle East respiratory syndrome coronavirus: quantification of the extent of the epidemic, surveillance biases, and transmissibility. *Lancet Infect. Dis.* **14** 50–56.
- CHAUMONT, L. and LIU, R. (2015). Coding multitype forests: Application to the law of the total population of branching forests. *Trans. Am. Math. Soc.* **368** 2723–2747.
- ENDO, A., ABBOTT, S., KUCHARSKI, A. J., FUNK, S. and CENTRE FOR THE MATHEMATICAL MODELLING OF INFECTIOUS DISEASES COVID-19 WORKING GROUP (2020). Estimating the overdispersion in COVID-19 transmission using outbreak sizes outside China. *Wellcome Open Res.* **5** 67.
- FARRINGTON, C. P., KANAAN, M. N. and GAY, N. J. (2003). Branching process models for surveillance of infectious diseases controlled by mass vaccination. *Biostatistics* **4** 279–295.
- GAY, N. J., DE SERRES, G., FARRINGTON, C. P., REDD, S. B. and PAPANIA, M. J. (2004). Assessment of the status of measles elimination from reported outbreaks: United States, 1997–1999. *J. Infect. Dis.* **189** Suppl 1 S36–42.
- GOOD, I. J. (1960). Generalizations to several variables of Lagrange’s expansion, with applications to stochastic processes. *Math. Proc. Camb. Philos. Soc.* **56** 367–380.
- HARRIS, T. E. (1963). *The theory of branching processes. Grundlehren der mathematischen Wissenschaften* **6**. Springer, Berlin, Germany.
- HART, W. S., BUCKINGHAM, J. M., KEITA, M., AHUKA-MUNDEKE, S., MAINI, P. K., POLONSKY, J. A. and THOMPSON, R. N. (2024). Optimizing the timing of an end-of-outbreak declaration: Ebola virus disease in the Democratic Republic of the Congo. *Sci. Adv.* **10** eado7576.
- HARTIG, F., MINUNNO, F. and PAUL, S. (2017). BayesianTools: General-purpose MCMC and SMC samplers and tools for Bayesian statistics. Title of the publication associated with this dataset: CRAN: Contributed Packages.
- HODCROFT, E. B., WOHLFENDER, M. S., NEHER, R. A., RIOU, J. and ALTHAUS, C. L. (2025). Estimating R_e and overdispersion in secondary cases from the size of identical sequence clusters of SARS-CoV-2. *PLoS Comput. Biol.* **21** e1012960.
- JAGERS, P. and LAGERÅS, A. (2008). General branching processes conditioned on extinction are still branching processes. *Electron. Commun. Probab.* **13** 540–547.
- KENAH, E. and ROBINS, J. M. (2007). Second look at the spread of epidemics on networks. *Phys. Rev. E Stat. Nonlin. Soft Matter Phys.* **76** 036113.
- KUCHARSKI, A. J. and ALTHAUS, C. L. (2015). The role of superspreading in Middle East respiratory syndrome coronavirus (MERS-CoV) transmission. *Euro Surveill.* **20** 14–18.
- KUCHARSKI, A. J. and EDMUNDS, W. J. (2015). Characterizing the transmission potential of zoonotic infections from minor outbreaks. *PLoS Comput. Biol.* **11** e1004154.
- LEE, H. and NISHIURA, H. (2019). Sexual transmission and the probability of an end of the Ebola virus disease epidemic. *Journal of Theoretical Biology* **471** 1–12.
- LEFEVRE, C. and PICARD, P. (1990). A non-standard family of polynomials and the final size distribution of Reed-Frost epidemic processes. *Adv. Appl. Probab.* **22** 25–48.
- LLOYD-SMITH, J. O., SCHREIBER, S. J., KOPP, P. E. and GETZ, W. M. (2005). Superspreading and the effect of individual variation on disease emergence. *Nature* **438** 355–359.
- MILLER, J. C. (2018). A primer on the use of probability generating functions in infectious disease modeling. *Infect. Dis. Model.* **3** 192–248.
- NISHIURA, H., YAN, P., SLEEMAN, C. K. and MODE, C. J. (2012). Estimating the transmission potential of supercritical processes based on the final size distribution of minor outbreaks. *J. Theor. Biol.* **294** 48–55.
- NISHIURA, H., MIYAMATSU, Y., CHOWELL, G. and SAITOH, M. (2015). Assessing the risk of observing multiple generations of Middle East respiratory syndrome (MERS) cases given an imported case. *Euro Surveill.* **20** 21181.
- NOCEDAL, J. and WRIGHT, S. J. (2006). *Numerical Optimization*, 1999 ed. *Springer Series in Operations Research and Financial Engineering*. Springer, New York, NY.
- PELLIS, L., BALL, F. and TRAPMAN, P. (2012). Reproduction numbers for epidemic models with households and other social structures. I. Definition and calculation of R_0 . *Math. Biosci.* **235** 85–97.

- QI, J., JU, W. and SUN, K. (2017). Estimating the propagation of interdependent cascading outages with multi-type branching processes. *IEEE Trans. Power Syst.* **32** 1212–1223.
- ROBERTS, D., JAMROZIK, E., HERIOT, G. S., SLIM, A. C., SELGELID, M. J. and MILLER, J. C. (2023). Quantifying the impact of individual and collective compliance with infection control measures for ethical public health policy. *Sci. Adv.* **9** eabn7153.
- SCALIA-TOMBA, G. (1990). On the asymptotic final size distribution of epidemics in heterogeneous populations. In *Stochastic Processes in Epidemic Theory* 189–196. Springer Berlin Heidelberg, Berlin, Heidelberg.
- SPENCER, S. E. F. and O’NEILL, P. D. (2011). The probability of containment for multitype branching process models for emerging epidemics. *J. Appl. Probab.* **48** 173–188.
- TRAN-KIEM, C. and BEDFORD, T. (2024). Estimating the reproduction number and transmission heterogeneity from the size distribution of clusters of identical pathogen sequences. *Proc. Natl. Acad. Sci. U. S. A.* **121** e2305299121.
- TREFETHEN, L. N. and WEIDEMAN, J. A. C. (2014). The exponentially convergent trapezoidal rule. *SIAM Rev. Soc. Ind. Appl. Math.* **56** 385–458.
- WAXMAN, D. and NOUVELLET, P. (2019). Sub- or supercritical transmissibilities in a finite disease outbreak: Symmetry in outbreak properties of a disease conditioned on extinction. *J. Theor. Biol.* **467** 80–86.

SUPPLEMENTARY MATERIAL FOR “COMPUTING THE FINAL EPIDEMIC SIZE DISTRIBUTIONS OF A MULTI-TYPE GALTON–WATSON PROCESS”

BY YUTA OKADA^{1,a} AND HIROSHI NISHIURA^{1,b}

¹*School of Public Health, Graduate School of Medicine, Kyoto University, okada.yuta.4y@kyoto-u.ac.jp;*
^b*nishiura.hiroshi.5r@kyoto-u.ac.jp*

1. Proof of Proposition 3.1. Restatement of Proposition 3.1:

Let $\mathbf{G}(z) = (G^{(1)}(z), \dots, G^{(n)}(z))^T$ be the offspring probability generating function (PGF) vector of an n -type Galton–Watson process (GWP) defined for $|z_i| \leq 1$, $i = 1, 2, \dots, n$, such that $\mathbf{J}_{\mathbf{G}}(\mathbf{r})$ has finite elements and is nonnegative and irreducible for $\mathbf{r} \in (0, 1]^n$. Then, there exists $\mathbf{r}^\# = (r_1^\#, \dots, r_n^\#) \in [0, 1]^n$ such that, for every complex vector \mathbf{z} inside the poly-disk $D_{\mathbf{z}} : |z_i| < r_i^\#, i = 1, \dots, n$, the functional equation

$$\mathbf{h} = \text{diag}(\mathbf{z})\mathbf{G}(\mathbf{h}) =: \mathbf{T}_{\mathbf{z}}(\mathbf{h})$$

has a unique solution $\mathbf{h} \in \mathbb{C}^n$ with $|\mathbf{h}| \leq |\mathbf{z}| < \mathbf{r}^\#$.

PROOF. First, by definition, the elements of both \mathbf{G} and its Jacobian matrix $\mathbf{J}_{\mathbf{G}}(\mathbf{z}) = \left[\left(\frac{\partial G^{(i)}}{\partial z_j} \right)_{i,j} \right] \in \mathbb{C}^{n \times n}$ are multivariate power series with nonnegative coefficients. Therefore, the following relationship holds for the weighted infinity norm by an arbitrary positive vector \mathbf{x} :

$$(1.1) \quad \|\mathbf{J}_{\mathbf{G}}(\mathbf{z})\|_{\infty, \mathbf{x}} \leq \|\mathbf{J}_{\mathbf{G}}(\mathbf{z})\|_{\infty, \mathbf{x}} \leq \|\mathbf{J}_{\mathbf{G}}(|\mathbf{z}|)\|_{\infty, \mathbf{x}},$$

where $\|\mathbf{A}\|_{\infty, \mathbf{x}} = \max_i \left(\frac{(\mathbf{A}\mathbf{x})_i}{x_i} \right)$. (Hereafter, we denote $|\mathbf{z}| = \mathbf{r} \in \mathbb{R}^n$.) Because $\mathbf{J}_{\mathbf{G}}(\mathbf{r})$ is nonnegative and irreducible, the Perron–Frobenius theorem implies that $\mathbf{J}_{\mathbf{G}}(\mathbf{r})$ has positive left and right leading eigenvectors $\mathbf{u}(\mathbf{r})$ and $\mathbf{v}(\mathbf{r})$ for every $\mathbf{r} = (r_1, \dots, r_n)$, $r_i \in (0, 1]$ (for simplicity, we assume $\mathbf{u}^T \mathbf{v} = 1$ without loss of generality) (Horn and Johnson, 2012). The elements of $\mathbf{J}_{\mathbf{G}}(\mathbf{r})$ and $\rho(\mathbf{J}_{\mathbf{G}}(\mathbf{r}))$, and the spectral radius of $\mathbf{J}_{\mathbf{G}}(\mathbf{r})$, are nondecreasing functions of \mathbf{r} .

Next, regarding $\mathbf{T}_{\mathbf{z}}(\mathbf{h})$, it readily follows that $|\mathbf{T}_{\mathbf{z}}(\mathbf{h})| < |\mathbf{z}| = \mathbf{r} \leq \mathbf{1}$ when $|\mathbf{h}| \leq |\mathbf{z}| = \mathbf{r} \leq \mathbf{1}$. Suppose we have \mathbf{h}, \mathbf{h}' such that $\mathbf{h} \neq \mathbf{h}'$ and $|\mathbf{h}| \leq |\mathbf{z}|, |\mathbf{h}'| \leq |\mathbf{z}|$. Here, we consider a linear path $\boldsymbol{\omega}(t) = \mathbf{h} + t(\mathbf{h}' - \mathbf{h})$, $t \in [0, 1]$. Note that $|\boldsymbol{\omega}(t)| \leq \max(|\mathbf{h}|, |\mathbf{h}'|) = \mathbf{r}$ and $|\mathbf{T}_{\mathbf{z}}(\boldsymbol{\omega}(t))| < |\mathbf{z}| \leq \mathbf{1}$. By writing $\mathbf{G}(\mathbf{h}') - \mathbf{G}(\mathbf{h})$ in the integral form as

$$(1.2) \quad \mathbf{G}(\mathbf{h}') - \mathbf{G}(\mathbf{h}) = \int_{t=0}^{t=1} \mathbf{J}_{\mathbf{G}}(\boldsymbol{\omega}(t))(\mathbf{h}' - \mathbf{h})dt,$$

Eq. (1.1) implies that the following relationship holds for an infinity norm weighted by an arbitrary positive vector \mathbf{x} :

$$(1.3) \quad \begin{aligned} \|\mathbf{G}(\mathbf{h}') - \mathbf{G}(\mathbf{h})\|_{\infty, \mathbf{x}} &\leq \left\| \int_{t=0}^{t=1} \mathbf{J}_{\mathbf{G}}(\boldsymbol{\omega}(t))(\mathbf{h}' - \mathbf{h})dt \right\|_{\infty, \mathbf{x}} \\ &\leq \int_{t=0}^{t=1} \|\mathbf{J}_{\mathbf{G}}(|\boldsymbol{\omega}(t)|)\|_{\infty, \mathbf{x}} \|\mathbf{h}' - \mathbf{h}\|_{\infty, \mathbf{x}} dt \\ &\leq \|\mathbf{J}_{\mathbf{G}}(\max(|\mathbf{h}|, |\mathbf{h}'|))\|_{\infty, \mathbf{x}} \|\mathbf{h}' - \mathbf{h}\|_{\infty, \mathbf{x}} \\ &\leq \|\mathbf{J}_{\mathbf{G}}(\mathbf{r})\|_{\infty, \mathbf{x}} \|\mathbf{h}' - \mathbf{h}\|_{\infty, \mathbf{x}}. \end{aligned}$$

Thus, it follows that

$$(1.4) \quad \|\mathbf{T}_z(\mathbf{h}') - \mathbf{T}_z(\mathbf{h})\|_{\infty, \mathbf{x}} \leq \|\text{diag}(\mathbf{r})\mathbf{J}_G(\mathbf{r})\|_{\infty, \mathbf{x}} \|\mathbf{h}' - \mathbf{h}\|_{\infty, \mathbf{x}}.$$

Setting $\mathbf{M}(\mathbf{r}) = \text{diag}(\mathbf{r})\mathbf{J}_G(\mathbf{r})$, we now show the existence of $\mathbf{r}^\# \in \mathbb{R}^n$ and $\mathbf{x} = \mathbf{x}(\mathbf{r}^\#) \in \mathbb{R}^n$ such that $\|\mathbf{M}(\mathbf{r}^\#)\|_{\infty, \mathbf{x}} < 1$ regardless of the criticality of \mathbf{G} .

(i) Subcritical case: $\rho(\mathbf{J}_G(\mathbf{1})) < 1$. It can be seen that $\rho(\mathbf{M}(\mathbf{r})) < 1$ for all $\mathbf{r} \in [0, 1]^n$, because $\mathbf{M}(\mathbf{r}) \leq \mathbf{J}_G(\mathbf{r}) \leq \mathbf{J}_G(\mathbf{1})$ holds element-wise. Therefore, by letting $\mathbf{x}(\mathbf{r}) = \mathbf{v}$ be the leading right eigenvector of $\mathbf{M}(\mathbf{r})$, $\|\mathbf{M}(\mathbf{r})\|_{\infty, \mathbf{v}} = \rho(\mathbf{M}(\mathbf{r})) < 1$.

(ii) Critical case: $\rho(\mathbf{J}_G(\mathbf{1})) = 1$. The same discussion as in (i) holds for all $\mathbf{r} \in [0, 1 - \epsilon]^n$.

(iii) Supercritical case: $\rho(\mathbf{J}_G(\mathbf{1})) > 1$. The vector of extinction probabilities $\mathbf{q} = (q_1, q_2, \dots, q_n) \in [0, 1]^n$ is the minimum real-valued solution of $\mathbf{q} = \mathbf{G}(\mathbf{q})$, and $\rho(\mathbf{J}_G(\mathbf{q})) < 1$. Here, for simplicity, we consider a linear path from \mathbf{q} to $\mathbf{1}$, $\mathbf{r}(t) = \mathbf{q} + t(\mathbf{1} - \mathbf{q})$, $t \in [0, 1]$. Because $\rho(\mathbf{M}(\mathbf{r}(0))) = \rho(\mathbf{M}(\mathbf{q})) < 1$ and $\rho(\mathbf{M}(\mathbf{r}(1))) = \rho(\mathbf{J}_G(\mathbf{1})) > 1$, there exist $t^* \in [0, 1]$ such that $\rho(\mathbf{M}(\mathbf{r}(t^*))) = 1$. Therefore, by choosing $\mathbf{r} = \mathbf{r}(t^* - \epsilon)$, it again follows that $\|\mathbf{M}(\mathbf{r})\|_{\infty, \mathbf{v}} = \rho(\mathbf{M}(\mathbf{r})) < 1$.

The discussion in (i)–(iii) ensures the existence of $\mathbf{r}^\#$ and $\mathbf{x} = \mathbf{v}(\mathbf{r}^\#)$ such that $\|\mathbf{M}(\mathbf{r})\|_{\infty, \mathbf{x}} < 1$. Therefore, the following holds for two vectors \mathbf{h} and \mathbf{h}' satisfying $|\mathbf{h}| \leq |\mathbf{z}|, |\mathbf{h}'| \leq |\mathbf{z}|$:

$$(1.5) \quad \|\mathbf{T}_z(\mathbf{h}') - \mathbf{T}_z(\mathbf{h})\|_{\infty, \mathbf{v}(\mathbf{r}^\#)} \leq L \|\mathbf{h}' - \mathbf{h}\|_{\infty, \mathbf{v}(\mathbf{r}^\#)},$$

where $L = \|\mathbf{M}(\mathbf{r})\|_{\infty, \mathbf{v}(\mathbf{r}^\#)} < 1$. Equation (1.5) ensures that, for a sequence $\mathbf{h}^{\{k\}}$ defined by $\mathbf{h}^{\{k+1\}} = \mathbf{T}_z(\mathbf{h}^{\{k\}})$, $\mathbf{h}^{\{0\}} \leq |\mathbf{z}| < \mathbf{r}^\#$, it follows that $\|\mathbf{h}^{\{k+1\}} - \mathbf{h}^{\{k\}}\|_{\infty, \mathbf{v}(\mathbf{r}^\#)}$ decreases geometrically as $k \rightarrow \infty$, ensuring the existence of $\lim_{k \rightarrow \infty} \mathbf{h}^{\{k\}} = \mathbf{h}^{\{\infty\}}$, the solution to the fixed-point equation $\mathbf{h} = \text{diag}(\mathbf{z})\mathbf{G}(\mathbf{h})$. Equation (1.5) also implies that $\mathbf{h}^{\{\infty\}}$ must be a unique solution. If two distinct vectors \mathbf{h}' and \mathbf{h}'' satisfying $|\mathbf{h}'| \leq |\mathbf{z}|, |\mathbf{h}''| \leq |\mathbf{z}|$ are the solutions to $\mathbf{h} = \mathbf{T}_z(\mathbf{h})$, applying \mathbf{T}_z to both vectors leads to

$$(1.6) \quad \|\mathbf{h}'' - \mathbf{h}'\|_{\infty, \mathbf{v}(\mathbf{r}^\#)} = \|\mathbf{T}_z(\mathbf{h}'') - \mathbf{T}_z(\mathbf{h}')\|_{\infty, \mathbf{v}(\mathbf{r}^\#)} \leq L \|\mathbf{h}'' - \mathbf{h}'\|_{\infty, \mathbf{v}(\mathbf{r}^\#)},$$

which can only happen when $\mathbf{h}'' = \mathbf{h}'$. Thus, there exists $\mathbf{r}^\#$ such that a unique solution exists in $|\mathbf{h}| \leq |\mathbf{z}| < \mathbf{r}^\#$ for $\mathbf{h} = \mathbf{T}_z(\mathbf{h})$. \square

2. Connection between the existence of derivatives and the choice of contour. As mentioned in the main text, the argument presented in the proof of Proposition 3.1 is essentially equivalent to choosing a domain for \mathbf{z} in which the derivatives of $\mathbf{H}(\mathbf{z})$ are finite.

Under the usual assumptions of Proposition 3.1, the derivatives of $\mathbf{G}(\mathbf{z})$ are analytic in $|\mathbf{z}| < \mathbf{r}^\#$. Implicit differentiation of $\mathbf{H}(\mathbf{z}) = \text{diag}(\mathbf{z})\mathbf{G}(\mathbf{H}(\mathbf{z}))$ with respect to \mathbf{z} then leads to

$$(2.1) \quad (\mathbf{I} - \text{diag}(\mathbf{z})\mathbf{J}_G(\mathbf{H})) \mathbf{J}_H(\mathbf{z}) = \text{diag}(\mathbf{G}(\mathbf{H})),$$

or

$$(2.2) \quad \mathbf{J}_H(\mathbf{z}) = (\mathbf{I} - \text{diag}(\mathbf{z})\mathbf{J}_G(\mathbf{H}))^{-1} \text{diag}(\mathbf{G}(\mathbf{H})).$$

The regularity of $\mathbf{I} - \text{diag}(\mathbf{z})\mathbf{J}_G(\mathbf{H})$ was discussed in the proof of Proposition 3.1. Therefore, as long as $|\mathbf{z}| < \mathbf{r}^\#$, the first-order derivative is finite, and it follows that $\mathbf{H}(\mathbf{z})$ is analytic in this region.

We can confirm this by iterative differentiation. Briefly, considering the m th-order derivative of $\mathbf{H}(\mathbf{z})$ that can be derived from iterative differentiation of $\mathbf{H}(\mathbf{z}) = \text{diag}(\mathbf{z})\mathbf{G}(\mathbf{H}(\mathbf{z}))$

with respect to an arbitrary sequence of variables $z_{l_1}, z_{l_2}, \dots, z_{l_m}$, by placing only the terms that have $\left[\frac{\partial^m \mathbf{H}}{\partial z_{l_1} \dots \partial z_{l_m}} \right] \in \mathbb{C}^n$ on the left hand side, we have that

$$(2.3) \quad (\mathbf{I} - \text{diag}(\mathbf{z})\mathbf{J}_G(\mathbf{H})) \left[\frac{\partial^m \mathbf{H}}{\partial z_{l_1} \dots \partial z_{l_m}} \right] = \mathbf{R}^{(m-1)}(\mathbf{z}),$$

where $\mathbf{R}^{(m-1)}(\mathbf{z}) \in \mathbb{C}^n$ denotes a vector consisting of terms with lower-order derivatives of $\mathbf{H}(\mathbf{z})$ and derivatives of $\mathbf{G}(\mathbf{z})$. This essentially means that $\mathbf{H}(\mathbf{z})$ is analytic, or that the derivatives of $\mathbf{H}(\mathbf{z})$ are finite and well-defined in $|\mathbf{z}| < \mathbf{r}^\#$.

3. Details on the numerical framework for calculation of the final size distribution.

3.1. *Cauchy integral calculation.* The evaluation of PGF coefficients by Cauchy integrals has previously been described in epidemiological contexts (Miller, 2018; Roberts et al., 2023). After choosing $\Gamma_{\mathbf{z}}$, in the main text, we evaluated the integrand of the Cauchy coefficient formula on multidimensional grids on $\Gamma_{\mathbf{z}}$ using DFT. As an example, for the two-dimensional cases we consider later, the grids are

$$(3.1) \quad \mathbf{z}(l_1, l_2; r_1, r_2) = (r_1 e^{2\pi i \frac{l_1}{N}}, r_2 e^{2\pi i \frac{l_2}{N}}), \quad l_1, l_2 = 0, \dots, N-1,$$

and the Cauchy integral can be approximated as

$$(3.2) \quad f^{(i)}(d_1, d_2) \approx \frac{1}{N^2} \sum_{l_1, l_2=0}^{N-1} \frac{h_i(\mathbf{z}(l_1, l_2; r_1, r_2))}{r_1^{d_1} r_2^{d_2}} \exp\left(-\frac{2\pi i}{N}(d_1 l_1 + d_2 l_2)\right).$$

In practice, we set the number of grids to $N = \max(2^5, 2^{\lceil \log_2(d_{\max}) \rceil + 1})$, where d_{\max} is the maximum degree in the dataset; this is a simple rule aligning with general recommendations to reduce aliasing errors while maintaining computational efficiency (Trefethen and Weideman, 2014; Cooley and Tukey, 1965).

3.2. *Solving the final size equation on the contour.* In the main text, we numerically solved $\mathbf{F}_{\mathbf{z}}(\mathbf{h}) = \mathbf{0}$ by minimizing the scalar function $\psi_{\mathbf{z}}(\mathbf{h}) = \|\mathbf{F}_{\mathbf{z}}(\mathbf{h})\|_2^2$, or the product of $\mathbf{F}_{\mathbf{z}}(\mathbf{h})$ and its conjugate transpose (note that $\psi_{\mathbf{z}}(\mathbf{h}) \geq 0$ by definition). Because the argument in Proposition 3.1 ensures the regularity of the Jacobian matrix $\mathbf{J}_{\mathbf{F}_{\mathbf{z}}}(\mathbf{h}) = \mathbf{I} - \text{diag}(\mathbf{z})\mathbf{J}_G(\mathbf{h})$ of $\mathbf{F}_{\mathbf{z}}$ when $|\mathbf{h}| \leq \mathbf{r}^\#$, we may choose a vector $\Delta(\mathbf{h}) = -\mathbf{J}_{\mathbf{F}_{\mathbf{z}}}^{-1}(\mathbf{h})\mathbf{F}_{\mathbf{z}}(\mathbf{h})$. The definition of $\Delta(\mathbf{h})$, for small $\alpha > 0$ means that $\psi_{\mathbf{z}}(\mathbf{h} + \alpha\Delta(\mathbf{h})) - \psi_{\mathbf{z}}(\mathbf{h}) \approx -2\alpha\psi_{\mathbf{z}}(\mathbf{h})$, and by letting $\alpha \rightarrow 0$, the directional differentiation can be written as

$$(3.3) \quad \frac{d}{d\alpha} \psi_{\mathbf{z}}(\mathbf{h} + \alpha\Delta(\mathbf{h}))|_{\alpha=0} = -2\psi_{\mathbf{z}}(\mathbf{h}).$$

As long as $\psi_{\mathbf{z}}(\mathbf{h}) > 0$, it follows that $\frac{d}{d\alpha} \psi_{\mathbf{z}}(\mathbf{h} + \alpha\Delta(\mathbf{h}))|_{\alpha=0} < 0$. Thus, we may compose an arbitrary sequence $\{\mathbf{h}^{(k)}\}$, $k = 0, 1, 2, \dots$ by Newton steps as follows:

$$(3.4) \quad \mathbf{h} \mapsto \mathbf{h} + \alpha\Delta(\mathbf{h}), \quad \Delta(\mathbf{h}) = -\mathbf{J}_{\mathbf{F}_{\mathbf{z}}}^{-1}(\mathbf{h})\mathbf{F}_{\mathbf{z}}(\mathbf{h}),$$

where $\mathbf{h}^{(0)}$ and $\alpha \in (0, 1]$ are chosen such that $|\mathbf{h}^{(k)}| < \mathbf{r}^\#$ and $\psi_{\mathbf{z}}(\mathbf{h} + \alpha\Delta(\mathbf{h})) < \psi_{\mathbf{z}}(\mathbf{h})$ for all $k \geq 0$. For simplicity, we can start the line search from $\alpha = 1$, and iterate the backtracking by $\alpha \mapsto \frac{\alpha}{2}$ up to five times; if $|\mathbf{h}^{(k)}| < \mathbf{r}^\#$ and $\psi_{\mathbf{z}}(\mathbf{h} + \alpha\Delta(\mathbf{h})) < \psi_{\mathbf{z}}(\mathbf{h})$ cannot be satisfied within five steps, we simply switch to a Picard step $\mathbf{h} \mapsto \mathbf{T}_{\mathbf{z}}(\mathbf{h})$. Because the sequence composed in this way converges to a unique solution for every \mathbf{z} on $\Gamma_{\mathbf{z}}$, as discussed in Proposition 3.1, we simply design the algorithm to start from $\mathbf{h}^{(0)} = \mathbf{0}$.

4. Numerical approach to ensure the validity of applying the Lagrange–Good formula. As described in the main text, the change-of-variables $z \mapsto \mathbf{h}$ involved in the Lagrange–Good Cauchy integral for the final size of multi-type GWPs is

$$(4.1) \quad z_i = \frac{h_i}{G^{(i)}(\mathbf{h})}, \quad i = 1, \dots, n,$$

where $G^{(i)}(\mathbf{h})$ is the offspring PGF of type i evaluated at \mathbf{h} :

$$(4.2) \quad G^{(i)}(\mathbf{h}) = \text{denom}_i(\mathbf{h})^{-k}, \quad \text{denom}_i(\mathbf{h}) = 1 + \frac{1}{k} \sum_{j=1}^n K_{ij}(1 - h_j).$$

The Jacobian matrix that accompanies this change of variables is

$$\mathbf{J}_{z \rightarrow \mathbf{h}}(\mathbf{h}) = \left[\frac{\partial z_i}{\partial h_j} \right],$$

where

$$(4.3) \quad \frac{\partial z_i}{\partial h_j} = \frac{1}{G^{(i)}(\mathbf{h})} \left(\delta_{ij} - \frac{h_i}{G^{(i)}(\mathbf{h})} \frac{\partial G^{(i)}(\mathbf{h})}{\partial h_j} \right).$$

We may factorize $\mathbf{J}_{z \rightarrow \mathbf{h}}(\mathbf{h})$ as

$$(4.4) \quad \mathbf{J}_{z \rightarrow \mathbf{h}}(\mathbf{h}) = \text{diag} \left(\frac{1}{G^{(1)}(\mathbf{h})}, \dots, \frac{1}{G^{(n)}(\mathbf{h})} \right) \mathbf{A}(\mathbf{h}), \quad A_{ij}(\mathbf{h}) = \delta_{ij} - \frac{h_i}{G^{(i)}(\mathbf{h})} \frac{\partial G^{(i)}(\mathbf{h})}{\partial h_j}.$$

Therefore,

$$\det(\mathbf{J}_{z \rightarrow \mathbf{h}}(\mathbf{h})) \neq 0 \iff \left(\prod_{i=1}^n G^{(i)}(\mathbf{h}) \neq 0 \right) \text{ and } \det(\mathbf{A}(\mathbf{h})) \neq 0.$$

Thus, for the numerical calculation of Lagrange–Good Cauchy integrals, we need to choose an integration contour $\Gamma_{\mathbf{h}}$ such that this condition is satisfied. In practice, extreme values of $|\det(\mathbf{J}(\mathbf{h}))|$ may lead to unstable numerical evaluation. Therefore, with a two-type case as an example, we select the polyradii $\mathbf{r} = (r_1, r_2)$ of

$$\Gamma_{\mathbf{h}} = C_{h_1}(r_1) \times C_{h_2}(r_2), \quad h_\ell = r_\ell e^{i\theta_\ell}, \quad \theta_\ell \in [0, 2\pi),$$

as follows. Let $\mathbf{q} = (q_1, q_2)$ be the extinction probability vector (smallest real solution of $\mathbf{q} = \mathbf{G}(\mathbf{q})$). Starting from the initial contour radii given by

$$(4.5) \quad r_\ell^{(0)} = \min\{(1 - \varepsilon_{\text{rad}})q_\ell, r_{\text{max}}\}, \quad \varepsilon_{\text{rad}} = 10^{-2}, \quad r_{\text{max}} = 0.95,$$

we then numerically approximate

$$m(\mathbf{r}) = \min_{\mathbf{h} \in \Gamma_{\mathbf{h}}} |\det(\mathbf{A}(\mathbf{h}))|$$

for parameters (t, θ_1, θ_2) with

$$(4.6) \quad \mathbf{h} = (t r_1^{(0)} e^{i\theta_1}, t r_2^{(0)} e^{i\theta_2}), \quad t \in [10^{-2}, 1], \quad \theta_1, \theta_2 \in [0, 2\pi),$$

under the constraint

$$(4.7) \quad |\text{denom}_i(\mathbf{h})| > 10^{-5}.$$

Given the resulting approximate minimum $\widehat{m}(\mathbf{r})$, we accept \mathbf{r} if $\widehat{m}(\mathbf{r}) > \tau_{\text{det}}$, where $\tau_{\text{det}} = 10^{-2}$. If the condition fails, we simply shrink the radius vector multiplicatively:

$$(4.8) \quad \mathbf{r} \leftarrow 0.9 \times \mathbf{r}$$

and repeat this process. The accepted radii are stored for each scenario.

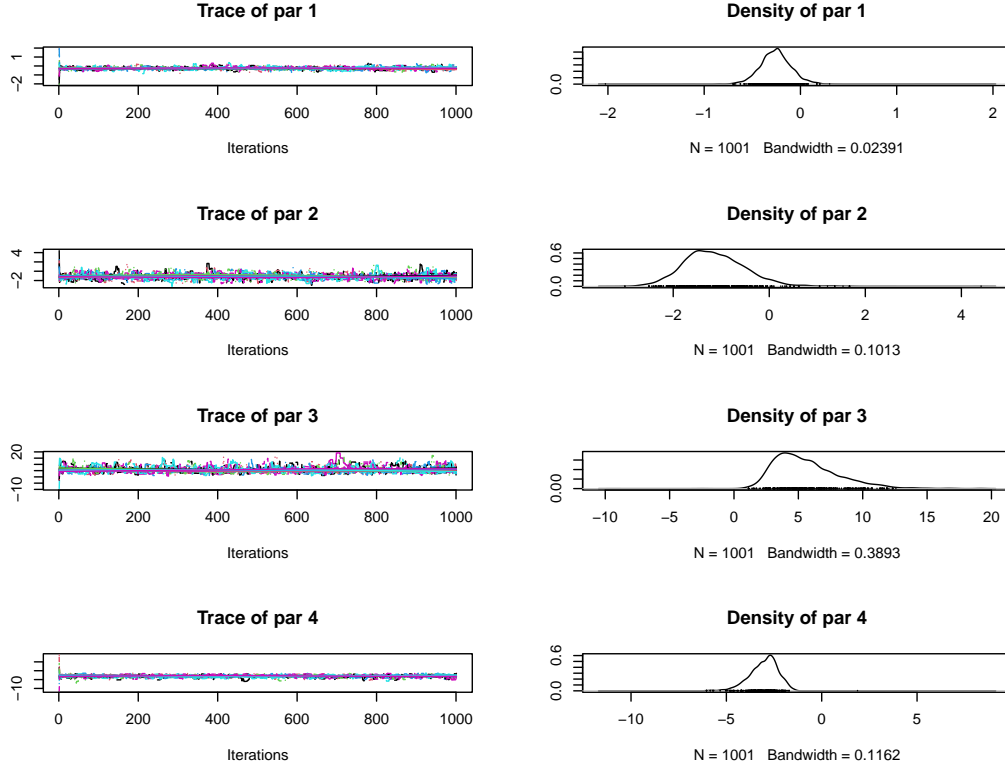


FIG S1. MCMC trace plots (left column) and marginal posterior density estimates (right column) for the model parameters.

5. Simulation of multi-type cluster data. We generated simulated cluster data from a two-type Galton–Watson branching process. For a type- $i \in \{1, 2\}$ infectious individual, the numbers of type-1 and type-2 secondary cases (X_{i1}, X_{i2}) follow a negative multinomial offspring distribution with a common dispersion parameter $k > 0$ and mean offspring matrix $\mathbf{K} = [(K_{ij})]$. Equivalently, conditional on the total number of secondary cases $X_i = X_{i1} + X_{i2}$, we draw $X_i \sim \text{NegBin}(\text{mean} = \sum_j K_{ij}, \text{size} = k)$, and then allocate secondary cases to types via a multinomial distribution with probabilities $K_{ij} / \sum_j K_{ij}$.

For each scenario, we simulated $n_1 = 20$ independent clusters with index type 1 and $n_2 = 20$ independent clusters with index type 2. Each cluster was simulated generation-by-generation starting from a single index case of the specified type, and the final size was recorded as (N_1, N_2) including the index case. The simulation was stopped when the process became extinct (no infectious individuals remained).

6. MCMC convergence diagnostics. Figure S1 displays the trace plots and density estimates, Figure S2 displays densities of prior and posterior distributions, and Figure S3 displays the correlation between model parameters. In all figures, parameters 1, 2, 3, 4 denote $\log R$, $\log k$, $\text{logit}(S)$, $\text{logit}(\pi)$, respectively.

7. Implicit differentiation of extinction probabilities by parameters of the negative multinomial distributions. Under the same assumptions on the offspring PGF as in Proposition 3.1, we start from the relationship $\mathbf{q} = \mathbf{G}(\mathbf{q})$ that the extinction probability vector $\mathbf{q} \in (0, 1)^n$ should satisfy. Here, $\mathbf{J}_{\mathbf{G}}(\mathbf{r})$ is assumed to have finite elements and is nonnegative and irreducible for $\mathbf{r} \in (0, 1]^n$.

Marginal parameter uncertainty

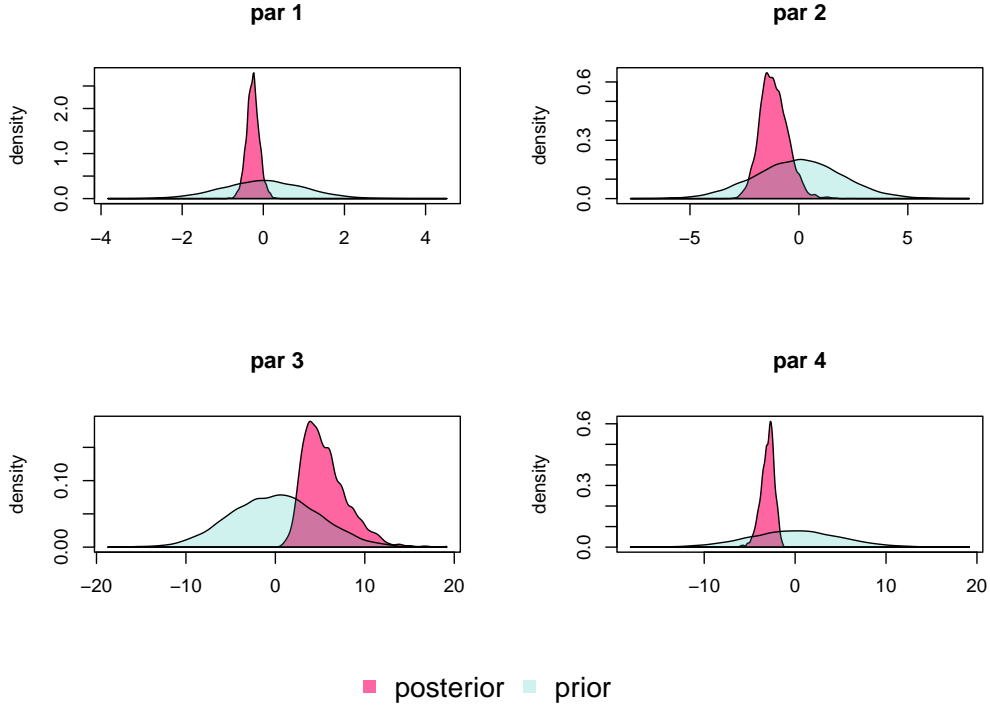


FIG S2. Overlay of prior and posterior densities for the model parameters. The light-blue shaded areas represent the prior distributions, whereas the red shaded areas represent the posterior distributions.

7.1. *Differentiation by elements of the mean offspring matrix.* A small perturbation of the mean offspring matrix $\mathbf{K} = \left[\frac{\partial G^{(i)}}{\partial z_j} \right]_{z=1}$ causes a small change in \mathbf{q} . For simplicity, we consider a perturbation of an arbitrary ℓ th column of the mean offspring matrix \mathbf{K} (which is essentially a $\mathbb{R}^{n \times n}$ slice of the entire change in \mathbf{q}) that lies in $\mathbb{R}^{n \times n \times n}$. We denote this perturbation to $\mathbf{K}_{\cdot \ell} = (K_{1\ell}, \dots, K_{n\ell})^\top$, the ℓ th column of \mathbf{K} , as $\Delta_{\mathbf{K}_{\cdot \ell}} = (\Delta_{K_{1\ell}}, \dots, \Delta_{K_{n\ell}})^\top$. The resulting change to $\mathbf{q} = \mathbf{G}(\mathbf{q})$ can then be written as

$$(7.1) \quad \left[\frac{\partial q_i}{\partial K_{j\ell}} \right] \Delta_{\mathbf{K}_{\cdot \ell}} = \left(\left[\frac{\partial G^{(i)}}{\partial K_{j\ell}} \right]_{z=\mathbf{q}} + \left[\frac{\partial G^{(i)}}{\partial z_j} \right]_{z=\mathbf{q}} \left[\frac{\partial q_i}{\partial K_{j\ell}} \right] \right) \Delta_{\mathbf{K}_{\cdot \ell}},$$

which leads to

$$(7.2) \quad \left(\mathbf{I} - \left[\frac{\partial G^{(i)}}{\partial z_j} \right]_{z=\mathbf{q}} \right) \left[\frac{\partial q_i}{\partial K_{j\ell}} \right] = \left[\frac{\partial G^{(i)}}{\partial K_{j\ell}} \right]_{z=\mathbf{q}}.$$

For $\mathbf{J}_{\mathbf{G}}(\mathbf{q}) = \left[\frac{\partial G^{(i)}}{\partial z_j} \right]_{z=\mathbf{q}}$, we know that $\rho(\mathbf{J}_{\mathbf{G}}(\mathbf{q})) < 1$. Therefore,

$$(7.3) \quad \left[\frac{\partial q_i}{\partial K_{j\ell}} \right] = \left(\sum_{m=0}^{\infty} \mathbf{J}_{\mathbf{G}}(\mathbf{q})^m \right) \left[\frac{\partial G^{(i)}}{\partial K_{j\ell}} \right]_{z=\mathbf{q}}.$$

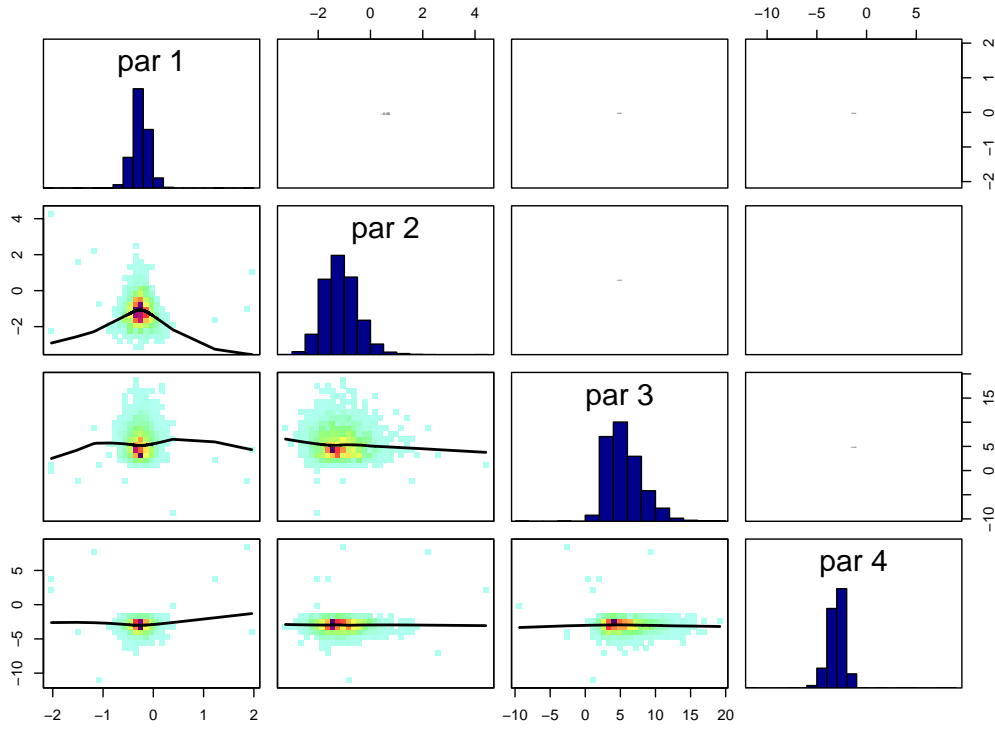


FIG S3. Posterior correlation plot for the MERS parameters.

On the right-hand side, $\sum_{m=0}^{\infty} \mathbf{J}_G(\mathbf{q})^m$ is a strictly positive matrix because $\mathbf{J}_G(\mathbf{q})$ is irreducible. For $\left[\frac{\partial G^{(i)}}{\partial K_{j\ell}} \right]_{\mathbf{z}=\mathbf{q}}$, we see that

$$(7.4) \quad \left. \frac{\partial G^{(i)}}{\partial K_{j\ell}} \right|_{\mathbf{z}=\mathbf{q}} = \begin{cases} -(1 - q_\ell) q_i^{1+1/k_i} < 0 & (i = j); \\ 0 & (i \neq j). \end{cases}$$

In summary, $\left[\frac{\partial q_i}{\partial K_{j\ell}} \right]$ is a product of a positive matrix and a negative diagonal matrix. Therefore, it follows that $\frac{\partial q_i}{\partial K_{j\ell}} < 0$.

7.2. Differentiation by overdispersion parameters. Similarly, we may consider a small perturbation vector $\Delta_{\mathbf{k}} = (\Delta_{k_1}, \dots, \Delta_{k_n})^\top$ added to \mathbf{k} . The change to $\mathbf{q} = \mathbf{G}(\mathbf{q})$ can be expressed as

$$(7.5) \quad \left[\frac{\partial q_i}{\partial k_j} \right] \Delta_{\mathbf{k}} = \left(\left[\frac{\partial G^{(i)}}{\partial k_j} \right]_{\mathbf{z}=\mathbf{q}} + \left[\frac{\partial G^{(i)}}{\partial z_j} \right]_{\mathbf{z}=\mathbf{q}} \left[\frac{\partial q_i}{\partial k_j} \right] \right) \Delta_{\mathbf{k}},$$

which leads to

$$(7.6) \quad \left(\mathbf{I} - \left[\frac{\partial G^{(i)}}{\partial z_j} \right]_{\mathbf{z}=\mathbf{q}} \right) \left[\frac{\partial q_i}{\partial k_j} \right] = \left[\frac{\partial G^{(i)}}{\partial k_j} \right]_{\mathbf{z}=\mathbf{q}}.$$

This can be rearranged as

$$(7.7) \quad \left[\frac{\partial q_i}{\partial k_j} \right] = \left(\sum_{m=0}^{\infty} \mathbf{J}_{\mathbf{G}}(\mathbf{q})^m \right) \left[\frac{\partial G^{(i)}}{\partial k_j} \right]_{\mathbf{z}=\mathbf{q}}.$$

Again, $\sum_{m=0}^{\infty} \mathbf{J}_{\mathbf{G}}(\mathbf{q})^m$ is a strictly positive matrix because $\mathbf{J}_{\mathbf{G}}(\mathbf{q})$ is irreducible. For $\left[\frac{\partial G^{(i)}}{\partial k_j} \right]_{\mathbf{z}=\mathbf{q}}$, $\frac{\partial G^{(i)}}{\partial k_j} = 0$ when $i \neq j$. For $i = j$,

$$(7.8) \quad \begin{aligned} \left. \frac{\partial \log G^{(i)}}{\partial k_i} \right|_{\mathbf{z}=\mathbf{q}} &= -\log \left(1 + \frac{1}{k_i} \sum_{m=1}^n K_{im} (1 - q_m) \right) + \frac{\frac{1}{k_i} \sum_{m=1}^n K_{im} (1 - q_m)}{1 + \frac{1}{k_i} \sum_{m=1}^n K_{im} (1 - q_m)} \\ &= \log(q_i^{1/k_i}) + 1 - q_i^{1/k_i}. \end{aligned}$$

The final line is strictly negative ($f(x) = 1 - x + \log(x)$ is a strictly increasing function of $x \in (0, 1)$ and $\lim_{x \rightarrow 1-0} f(x) = 0$). Therefore, $\left[\frac{\partial G^{(i)}}{\partial k_j} \right]_{\mathbf{z}=\mathbf{q}}$ is a matrix with negative diagonal elements, and it follows that $\frac{\partial q_i}{\partial k_j} < 0$.

Acknowledgments. Hiroshi Nishiura is also affiliated with the Center for Health Security, Graduate School of Medicine, Kyoto University.

REFERENCES

- COOLEY, J. W. and TUKEY, J. W. (1965). An algorithm for the machine calculation of complex Fourier series. *Math. Comput.* **19** 297.
- HORN, R. A. and JOHNSON, C. R. (2012). *Matrix Analysis*, 2 ed. Cambridge University Press, Cambridge, England.
- MILLER, J. C. (2018). A primer on the use of probability generating functions in infectious disease modeling. *Infect. Dis. Model.* **3** 192–248.
- ROBERTS, D., JAMROZIK, E., HERIOT, G. S., SLIM, A. C., SELGELID, M. J. and MILLER, J. C. (2023). Quantifying the impact of individual and collective compliance with infection control measures for ethical public health policy. *Sci. Adv.* **9** eabn7153.
- TREFETHEN, L. N. and WEIDEMAN, J. A. C. (2014). The exponentially convergent trapezoidal rule. *SIAM Rev. Soc. Ind. Appl. Math.* **56** 385–458.